5-4-2018

Charge and Bonding in CuGeO3 Nanorods

Kenneth Robert O'Neal
koneal5@vols.utk.edu

Amal al-Wahish
University of Tennessee, Knoxville

Z-Q Li
Hefei Institues of Physical Sciences

G Dhalenne
Universite Paris-Sud

A Revcolevschi
Universite Paris Sud (Paris XI)

See next page for additional authors

Charge and Bonding in $CuGeO_3$ Nanorods

Kenneth R. O'Neal,[†] Amal al-Wahish,[†] Zhao-Qian Li,[‡] Guy Dhalenne,[¶] Alexandre Revcolevschi,[¶] Xue-Tai Chen,[§] and Janice L. Musfeldt[*,†]

†*Department of Chemistry, University of Tennessee, Knoxville, Tennessee 37996, USA*

‡*Institute of Applied Technology, Hefei Institutes of Physical Science, Chinese Academy of Sciences, Hefei, Anhui 230031, PR China*

¶*SP2M-ICMMO UMR-CNRS 8182, Université Paris-Sud, 91405 Orsay Cedex, France*

§*State Key Laboratory of Coordination Chemistry, Nanjing National Laboratory of Microstructures, School of Chemistry and Chemical Engineering, Nanjing University, 210023, PR China*

‖*Department of Physics and Astronomy, University of Tennessee, Knoxville, Tennessee 37996, USA*

E-mail: musfeldt@utk.edu

Abstract

We combine infrared and Raman spectroscopies to investigate finite length scale effects in $CuGeO_3$ nanorods. The infrared-active phonons display remarkably strong size dependence whereas the Raman-active features are, by comparison, nearly rigid. A splitting analysis of the Davydov pairs reveals complex changes in chemical bonding with rod length and temperature. Near the spin-Peierls transition, stronger intralayer bonding in the smallest rods indicates a more rigid lattice which helps to suppress the spin-Peierls transition. Taken together, these findings advance the understanding of size effects and collective phase transitions in low-dimensional oxides.

KEYWORDS: spin-Peierls transition, magnetoelastic coupling, size effects, phonon confinement, nanorods, vibrational spectroscopy

Table of contents graphic

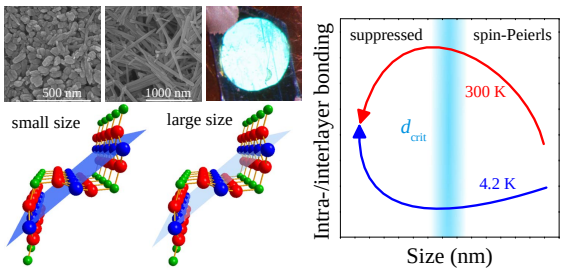

Phase transitions in nanomaterials are a subject of contemporary interest. This is because of the remarkable mechanistic diversity in how size enables the development of new states of matter,[1,2] disrupts one transition in favor of another,[3,4] or blocks the development of collective phenomena entirely.[5,6] One example of a transition with emergent properties is that of oxides such as $BiFeO_3$, where the nanoparticles display a ferroelectric $\rightarrow$ paraelectric crossover with decreasing size.[7] The development of the super-paramagnetic state in $CoFe_2O_4$ and $MgFe_2O_4$ nanoparticles is another illustration of how size allows access to completely different properties and areas of phase space.[8,9] Other examples include the spin-flop transition in α-Fe_2O_3 that is suppressed below approximately 8 nm[10,11] and magnetoelectric coupling in Fe_3O_4, which is reduced with decreasing size.[12] The discovery of size-induced quenching of the spin-Peierls transition in nanoscale $CuGeO_3$[13,14] is another case where collective phenomena are suppressed by length scale effects. That the spin-Peierls state can be switched with both temperature and size is intriguing and merits additional mechanistic investigation.

$CuGeO_3$ is well known as the first inorganic spin-Peierls material[15] and, as such, is a superb platform for exploring temperature,[16–19] magnetic field,[20–25] pressure,[26–29] and doping effects.[30–33] This system consists of edge-sharing CuO_6 octahedra that form quasi-one-dimensional chains along the crystallographic c axis (Fig. 1 (a)).[18,34] The Cu centers are d^9 and therefore S=1/2. The Cu atoms dimerize below the T_{SP}=14 K spin-Peierls transition,[15] and spin gaps open because singlets are formed.[15,35] Vibrational spectroscopies reveal the coupled phonons.[18,36–40] The recent development of a suite of $CuGeO_3$ nanorods of different lengths[13] (Fig. 1 (b-d)) offers the opportunity to unravel size effects on the dynamic properties and, at the same time, explore how and why the spin-Peierls transition is suppressed below a critical size ($d_{crit} \approx 450$ nm).[13,14] Electron spin resonance reveals no sign of an antiferromagnetic state at small sizes,[14] contrary to expectations based upon chemical substitution with Si, Zn, and Mg.[41–43] Instead, disorder emanating from the small surface layer and local changes in the Cu–O–Cu superexchange pathway that increase interchain interactions may place $CuGeO_3$ nanorods in the vicinity of a disorder-driven quantum critical point.[14]

In this work, we reach beyond temperature, magnetic field, and pressure tuning techniques to explore the vibrational properties of $CuGeO_3$ nanorods as a function of size. An additional and rather novel aspect of our approach is that while all nanorod diameters are similar, the growth habit is such that length can be controlled to vary confinement in the c direction (Figs. 1 (b-d)).[13] Strikingly, the infrared-active modes show dramatic size effects whereas the Raman-active features are nearly rigid. A Davydov splitting analysis reveals an overall higher intra- to interlayer bonding ratio in the nanorods as compared to the bulk, likely due to enhancement of bc-plane dimensionality. Importantly, at temperatures near the spin-Peierls transition, the intralayer bonding goes through a weak minimum near d_{crit} and then turns sharply upward with decreasing size. This indicates a lattice that is stiffer and more difficult to dimerize, consistent with the suppression of the spin-Peierls transition at small sizes.[13,14] Taken together, these findings advance the understanding of size-driven

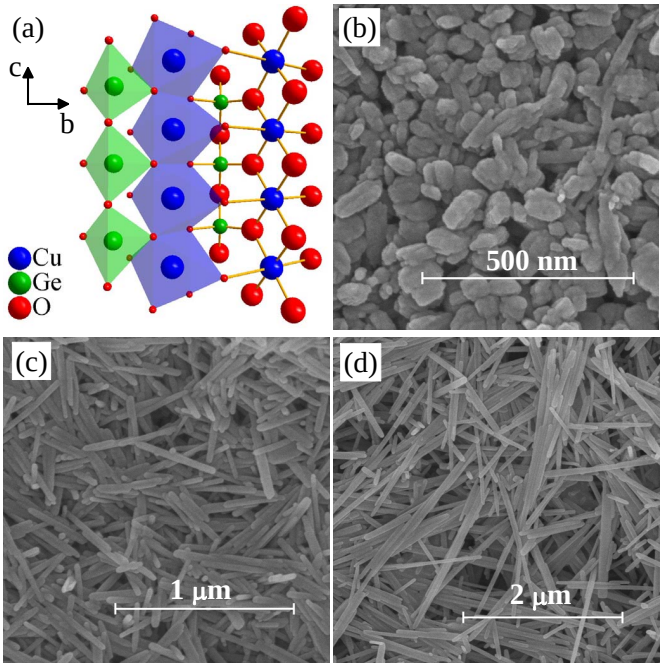

Figure 1: (a) 300 K crystal structure of $CuGeO_3$ showing the Cu chains along the c axis.[18,34] The space group is *Pbmm*. (b-d) Scanning electron microscope images of representative nanorods studied in this work. All samples have diameters near 50 nm but varying lengths. These images show nanorods with average lengths of (b) 150 nm, (c) 400 nm, and (d) greater than 1000 nm.

phase transitions in nanoscale transition metal oxides and place these materials on a firm foundation for future work in high magnetic field. They also reveal how phonon size effects may be important for catalysis, thermal conductivity, and sensing applications.

Size-dependent vibrational properties of $CuGeO_3$ nanorods

Figure 2 displays the infrared and Raman scattering response of $CuGeO_3$ as a function of size at 300 K. The spectral features are in reasonable agreement with prior single crystal measurements,[44,45] so we adopt earlier mode assignments[30] and displacement patterns[45] to describe the lattice dynamics of the nanorods. Within this framework, features below 250 cm^{-1} are related to copper and germanium motion whereas those above 250 cm^{-1} contain mostly oxygen displacement.[45] Only a few phonons are important to the 14 K spin-Peierls transition in the single crystal. These include the infrared-active B_{3u} mode near 295 cm^{-1},[38,39]

an infrared-active folded zone-boundary mode near 800 cm^{-1},[40] and the Raman-active B_{3g} and B_{2g} modes at 110 cm^{-1} and 222 cm^{-1}, respectively.[36] Our initial expectation was that this short list of coupled phonon modes would display signatures of important size-induced changes to the lattice. For example, mode disappearance, splitting, or sudden frequency shifts across the 450 nm critical length scale could indicate the inability of the lattice to dimerize at low temperatures. Upon examination, however, these modes do not seem to be of particular importance to the size-induced suppression of the spin-Peierls transition. The actual situation is more subtle and requires close analysis, as detailed below.

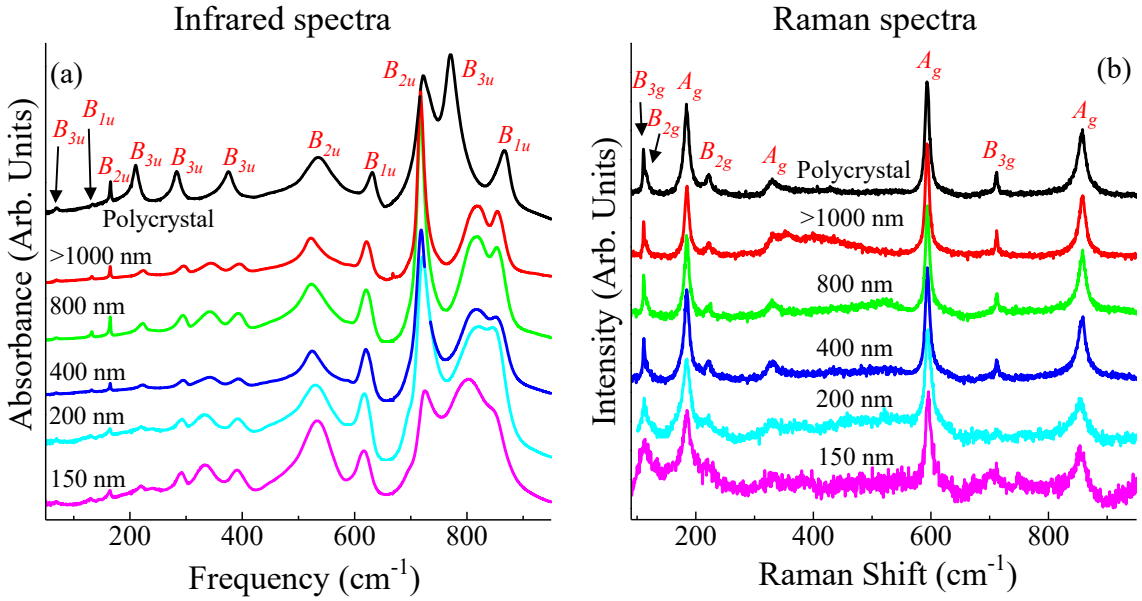

Figure 2: (a) Infrared and (b) Raman spectra of $CuGeO_3$ polycrystal and nanorods of various lengths as indicated. Mode symmetries are labeled based on assignments for the bulk material.[46] All polarizations are observed simultaneously due to the random orientation intrinsic to nanomaterials, although the phonons retain their directional character as indicated by the assignments.[30,46] Surface disorder and size distributions increase linewidth in several of the modes as well.[14]

Figure 3 displays frequency vs. size trends for several representative infrared-active modes at different temperatures above and below T_{SP}. A full accounting of the infrared features is available in Fig. S3. Overall, phonons corresponding to Cu and Ge motions (below 250 cm^{-1}) display weak frequency shifts with decreasing size (Fig. 3 (a-c)), whereas those involving oxygen motion exhibit much stronger changes (Fig. 3 (d-f)). We distinguish two

different types of size effects: (i) a sharp frequency jump going from polycrystal to nanorod that represents confinement perpendicular to the length of the nanorod and (ii) the frequency shift as nanorod length decreases, which correlates to changes along the c axis. These trends are discussed below.

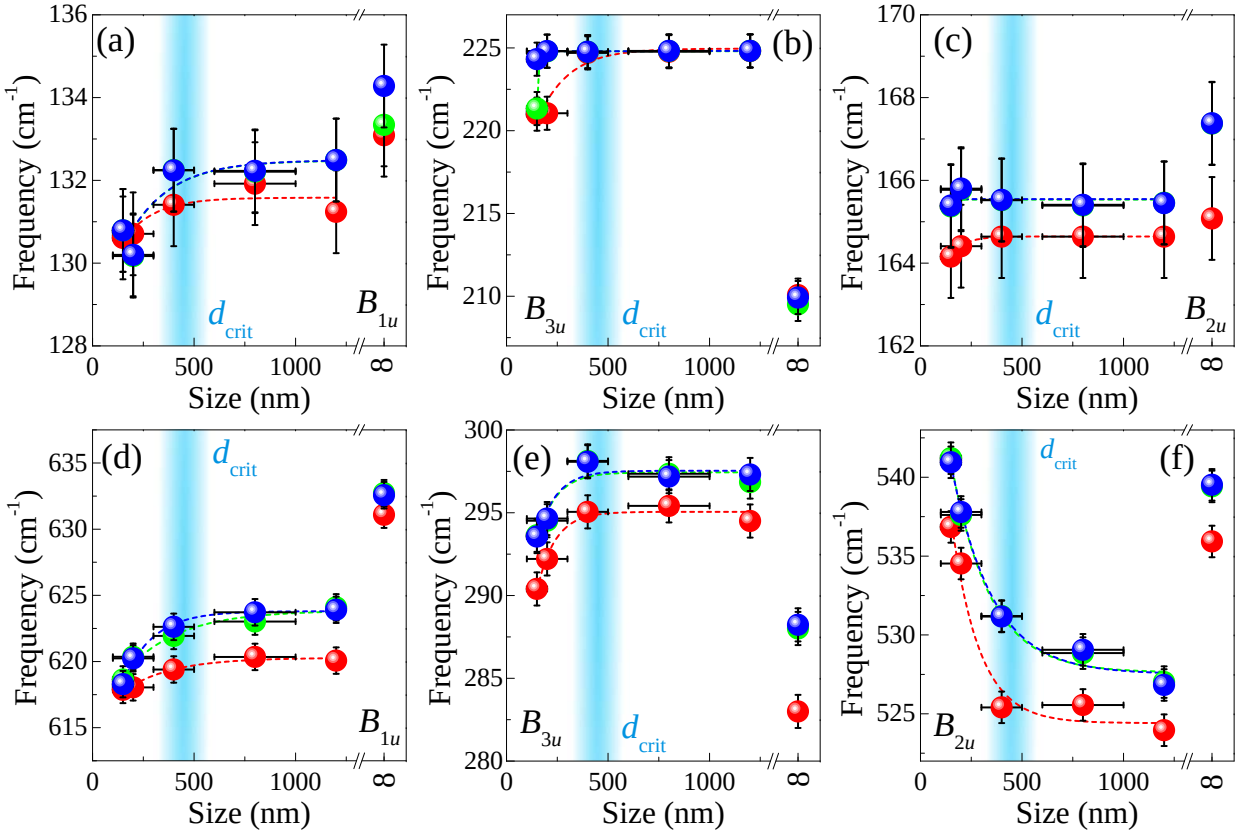

Figure 3: Frequency vs. size at 300 K (red), 20 K (green), and 4.2 K (blue) for representative infrared modes of $CuGeO_3$ with the indicated symmetries as approximated from single crystal studies.[45] (a-c) Modes below 250 cm^{-1} show only a weak size dependence whereas (d-f) the higher frequency modes display larger frequency shifts. Here, we use infinite size to indicate the polycrystalline bulk material. The vertical shaded region represents the critical length scale d_{crit} for suppression of the low temperature spin-Peierls transition. Dashed lines guide the eye.

We first examine *ab* plane size effects. We do this by realizing that the growth habit of the $CuGeO_3$ nanorods is such that the diameter is always ≈50 nm, within the range of phonon confinement for some oxides.[47,48] Differences in the infrared response of the polycrystal and largest nanorod sample (which is longer than 1000 nm) can therefore be attributed to finite length scale effects within the *ab* plane. As expected, phonons polarized along these

directions display sizable frequency shifts (up to 55 cm^{-1}, see Fig. S3), although these shifts occur in different directions (Fig. 3 (d,e) for example). In general, modes polarized along a (B_{1u}) soften across the bulk to 1000 nm nanorod size range, whereas b-directed (B_{3u}) phonons harden. The latter is consistent with overall stronger interchain interactions in the nanorods. Interestingly, the c-polarized (B_{2u}) modes are also sensitive to this two-dimensional confinement and soften (Fig. 3 (f)), even though the length of the longest nanorods (along the c axis) is well above the length scale where finite size effects strongly affect phonon energies.[7,47,49]

We now turn our attention to the infrared response of $CuGeO_3$ as a function of size. Here, plots of frequency vs. size characterize trends that develop as a function of the nanorod length (along the c axis) while keeping diameter fixed.[13] One might anticipate that reducing nanorod length will affect only c-directed modes. As shown in Fig. 3, this is clearly not the case. There are, however, consistent directional trends. For instance, both a- and b-polarized modes red shift with decreasing size, while the c-polarized (B_{2u}) modes harden. The overall spectral character is similar above and below d_{crit}, with the frequency shifts of interest occurring across 450 nm. Remarkably, the lattice is sensitive to this critical length scale even at room temperature.

Figure 4 displays frequency vs. size for several representative Raman features at different temperatures. The size dependence of the Raman-active modes in nanoscale $CuGeO_3$ is considerably weaker than that of the infrared-active phonons. Most modes display only small frequency shifts regardless of symmetry. This is true both for the jump from polycrystal to longest nanorod (a maximum of 1 cm^{-1} for Raman modes compared to 55 cm^{-1} in the infrared) and the dependence on nanorod length (as high as 11 cm^{-1} for the 116 cm^{-1} Raman mode vs. 20 cm^{-1} for the 772 cm^{-1} infrared mode). There are no consistent hardening or softening trends within a particular symmetry. As in the infrared features, most modes begin to display confinement effects below $d_{crit} \approx 450$ nm - even though the changes are not so large - while others are entirely rigid across this size regime. Again, modes harden at low temperature, although the overall shifts are smaller than the infrared phonons.

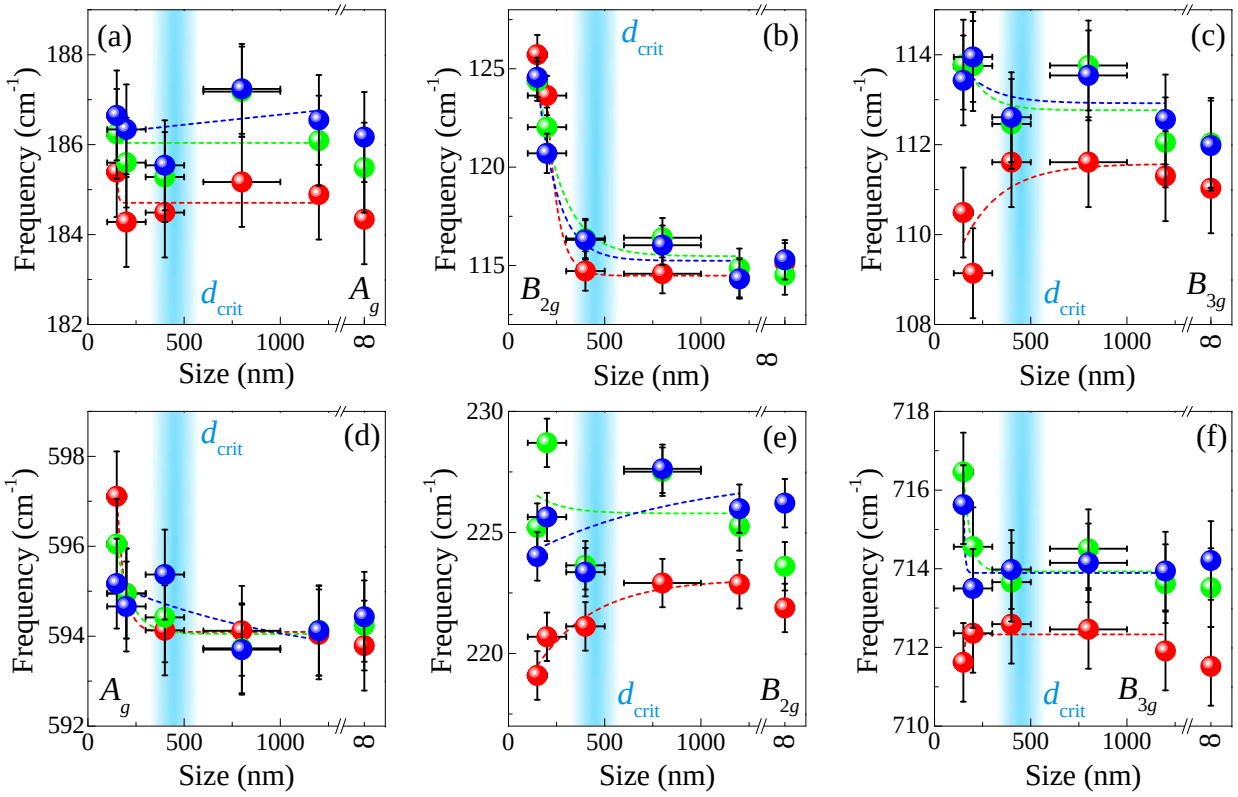

Figure 4: (a-f) Frequency vs. size at 300 K (red), 20 K (green), and 4.2 K (blue) for representative Raman modes of $CuGeO_3$ with the indicated symmetries as approximated from single crystal studies.[45] Note that the frequency scales on the y axes are much smaller than those in Fig. 3 in order to visualize the smaller frequency shifts. The vertical shaded region represents the critical length scale d_{crit} for suppression of the low temperature spin-Peierls transition. Dashed lines guide the eye.

Evaluating intra- vs. interlayer bonding strength

Infrared phonons are exquisitely sensitive to charge and bonding because they directly probe charge on the potential surface.[50,51] One way to quantify this effect, assuming size-induced changes to the structure and stoichiometry can be ruled out as was done here,[52] is by evaluating chemical bond strength. In materials with multiple formula units per unit cell, this is accomplished with an analysis of the Davydov splitting that arises from the interaction of neighboring formula units.[45,46,53,54] In our case, the unit cell of $CuGeO_3$ contains two formula units[34] which splits the 218, 330, 403, 605, 716, and 851 cm^{-1} modes into Davydov pairs (Fig. 5 (a), for example).[45] Each pair consists of independent infrared and Raman

branches that are split from a central unperturbed frequency. Comparing the frequencies of the infrared and Raman components of the Davydov pairs allows for an analysis of the relative strength of intra- vs. interlayer bonding.[45] We employ this framework to evaluate bonding strength trends in this suite of nanorods.

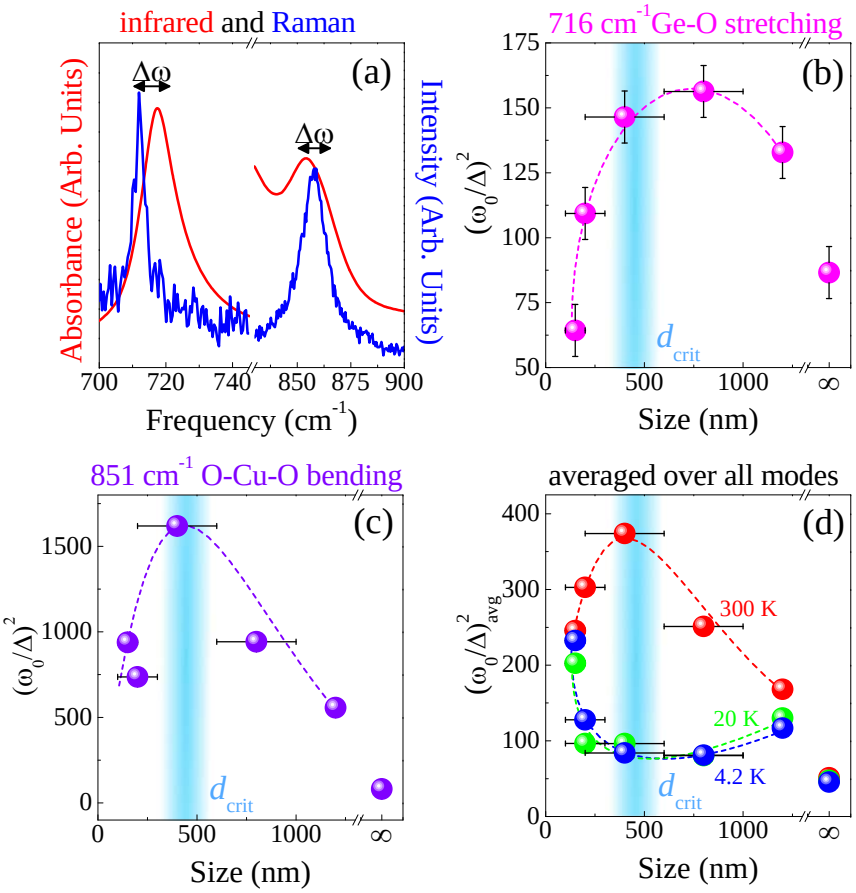

Figure 5: (a) Close-up views of the infrared (red) and Raman (blue) spectra of representative Davydov doublets in the longest nanorods at 300 K. $(\omega_0/\Delta)^2$ vs. size as determined from the (b) 716 and (c) 851 cm^{-1} pairs. (d) Averaging over all Davydov pairs yields $(\omega_0/\Delta)^2_{avg}$ vs. size, representing the size dependence of intra- vs. interlayer bonding strength for $CuGeO_3$ at 300 (red), 20 (green) and 4.2 K (blue). The vertical shaded region represents the critical length scale d_{crit} below which the spin-Peierls transition is quenched. Dashed lines guide the eye.

We observe the majority of known Davydov pairs[45] in the $CuGeO_3$ nanorods, supporting a comprehensive analysis of the mode splittings to reveal size-induced changes in bonding. The infrared and Raman branch frequencies (for each pair) are defined as ω_+ and ω_-, respectively. We then calculate $(\omega_0/\Delta)^2$, which represents the ratio of intralayer to interlayer

bonding strength, from the relation $\omega_{\pm} = (\omega_0^2 \pm \Delta^2)^{1/2}$ which is valid for a pair of weakly coupled identical oscillators.[46,54,55] Here, ω_0 is the isolated (unperturbed) oscillator frequency, and Δ^2 is proportional to the coupling force constant.[46,54,55] Tables 1 and 2 summarize this analysis for the doublets centered at 716 and 851 cm^{-1}. As a reminder, these modes are assigned as oxygen stretching around Ge and Cu, respectively.[30,45] Tables S2-4 summarize the results for other pairs. Comparing $(\omega_0/\Delta)^2$ as determined for individual Davydov pairs as a function of size (Fig. 5 (b,c)) reveals that, yet again, there is a clear difference between the polycrystal and the longest nanorod. Charge and bonding also depends strongly on nanorod length. At 300 K, $(\omega_0/\Delta)^2$ rises - reaching a maximum near d_{crit} - and drops again at smaller size.

Table 1: Summary of the 300 K Davydov splitting analysis for the 716 cm^{-1} pair carried out for the $CuGeO_3$ polycrystal and nanorods. Here, ω_+, ω_-, and ω_0 are the infrared, Raman, and unperturbed frequencies, respectively, Δ is proportional to the weak coupling between interacting identical oscillators, and $(\omega_0/\Delta)^2$ is proportional to the intra-vs.-interlayer bonding strength.

Sample	ω_+ (cm^{-1})	ω_- (cm^{-1})	ω_0 (cm^{-1})	Δ	$(\omega_0/\Delta)^2$
polycrystal	711.5	719.8	715.7	76.9	86.6
over 1000 nm	711.9	717.3	714.6	62.0	132.8
800 nm	712.5	717.0	714.6	57.2	156.3
400 nm	712.6	717.5	715.0	59.1	146.5
200 nm	712.4	718.9	715.6	68.4	109.3
150 nm	711.6	722.8	717.2	89.5	64.3

Table 2: Summary of the 300 K Davydov splitting analysis for the 851 cm^{-1} pair carried out for the $CuGeO_3$ polycrystal and nanorods. Here, ω_+, ω_-, and ω_0 are the infrared, Raman, and unperturbed frequencies, respectively, Δ is proportional to the weak coupling between interacting identical oscillators, and $(\omega_0/\Delta)^2$ is proportional to the intra-vs.-interlayer bonding strength.

Sample	ω_+ (cm^{-1})	ω_- (cm^{-1})	ω_0 (cm^{-1})	Δ	$(\omega_0/\Delta)^2$
polycrystal	857.0	867.6	862.3	95.7	81.2
over 1000 nm	857.6	856.0	856.8	36.6	556.6
800 nm	857.5	856.5	857.0	27.9	942.0
400 nm	857.3	858.4	858.1	21.3	1618.8
200 nm	854.1	855.2	854.7	31.5	736.5
150 nm	853.9	854.8	854.4	27.9	938.6

Averaging $(\omega_0/\Delta)^2$ over all Davydov pairs allows for a more robust comparison between $CuGeO_3$ polycrystal and nanorods. Carrying out this analysis at 300, 20, and 4.2 K reveals surprising trends (Fig. 5 (d)). Starting with the polycrystal data, we see that temperature effects are quite small, benchmarking thermal contraction effects. Such small changes are reasonable based on unit cell parameter trends in single crystals:[18] b decreases, c increases, and a is nearly constant with decreasing temperature. Thermal effects are much stronger in the nanorods, an indication that traditional contraction effects are amplified - possibly due to enhanced interchain interactions.

Looking at the 300 K data, we observe strong size effects on $(\omega_0/\Delta)^2_{avg}$ (Fig. 5 (d)). With decreasing rod length, $(\omega_0/\Delta)^2_{avg}$ reaches a maximum at d_{crit} then decreases, indicating that the lattice is sensitive to this critical length scale even far away from T_{SP} and the onset of magnetic ordering. Since the interlayer bonds are along a and the nanorod length (which varies) is along c,[13] we surmise that the main driver of modifications to $(\omega_0/\Delta)^2_{avg}$ arises from changes in intralayer (bc-plane) bonding at small sizes. This change in bonding strength explains the large frequency shifts of infrared modes as compared to Raman analogs. Interestingly, the size-dependent trend at low temperature is quite different from that at 300 K. Instead of reaching a maximum, $(\omega_0/\Delta)^2_{avg}$ goes through a weak minimum near d_{crit} and sharply rises at smaller sizes. Similar trends are observed at both 20 and 4.2 K. This indicates that the intralayer bonding strengthens at small sizes, which may be responsible for the suppression of the spin-Peierls transition.

Mechanism of the size-induced quenching of the spin-Peierls transition

The spin-Peierls transition is a cooperative distortion that arises when a quasi-one-dimensional spin chain interacts with surrounding phonons.[56] When it is blocked (as in the shortest nanorods of interest here), both the spin and lattice channels must be examined to determine the suppression mechanism. The microscopic nature of the coupling phonons in

$CuGeO_3$ is well-known,[18,36–40] providing candidates with which to explore the role of the lattice. With the exception of the 800 cm^{-1} folded zone-boundary phonon, these features appear in our spectra. While there are no dramatic changes such as mode disappearance or splitting near 450 nm, the large frequency shifts below this length scale seem to signal important changes in chemical bonding and dimensionality.

As discussed above, $(\omega_0/\Delta)^2_{avg}$ from the complete Davydov analysis provides a framework within which we can compare overall chemical bonding trends in this set of materials. Figure 5 (d) shows that $(\omega_0/\Delta)^2_{avg}$ is everywhere higher in the nanorods as compared to the polycrystal. This means that intralayer bonding is stronger - regardless of nanorod length. Such increased stiffness makes it more difficult to dimerize the Cu centers, weakening the spin-Peierls transition in the longer nanorods.[13] In other words, at smaller size scales, the intralayer bonding is stronger than the interlayer bonding, leading to an energetic barrier to the dimerization process typically required for a spin-Peierls transition. At low temperature, $(\omega_0/\Delta)^2_{avg}$ rises sharply below d_{crit}. This further increase in rigidity works to increase interchain interactions and block the spin-Peierls transition below $d_{crit} \approx 450$ nm. External stimuli such as strain may have similar effects on stiffness and dimerization and should be explored for property control.

In summary, we measured the spectroscopic response of nanoscale $CuGeO_3$ in order to explore size effects. We find that infrared phonons display strong frequency shifts with decreasing size whereas the Raman modes are nearly rigid - trends that a Davydov splitting analysis attributes to changes in chemical bonding. At low temperature, the intralayer bonding is strengthened below d_{crit} such that the lattice may not be able to dimerize, thereby blocking the spin-Peierls transition. These findings advance the understanding of cooperative phase transitions and size effects in low-dimensional oxides.

Methods

$CuGeO_3$ nanorods were prepared by hydrothermal methods as described previously[13] and characterized using scanning electron microscopy and x-ray diffraction (Figs. 1 and S1). Polycrystalline samples were prepared for comparison by floating zone techniques using an image furnace.[57] Samples were mixed with a transparent matrix (paraffin or KBr) to form pressed pellets. Infrared transmittance measurements (20-2,000 cm^{-1}, 1-4 cm^{-1} resolution) were carried out with Bruker 113v and Equinox 55 spectrometers. Absorption was calculated as $\alpha(\omega) = \frac{-1}{hd} ln(T(\omega))$, where h is sample loading, d is thickness, and $T(\omega)$ is measured transmittance. Raman spectra (70-1000 cm^{-1}) of powders were acquired with an 1800g/mm grating, integration times of 60 seconds, and averaged three times. The larger sizes were measured using a 532 nm laser with a power of 25 mW, while for the smallest sizes a 473 nm laser[58,59] with power below 5 mW was employed to prevent sample degradation. Temperature control was achieved with an open flow helium cryostat (4.2-300 K). Standard peak fitting procedures were employed as appropriate.

Acknowledgments

Research at the University of Tennessee is supported by the Materials Science Division, Office of Basic Energy Sciences, U.S. Department of Energy under Award DE-FG02-01ER45885. We thank Lei Chen and Ziling Xue for useful discussions.

Supporting information

Supporting information is available including details of nanorod synthesis and characterization, vibrational mode assignments, size-dependent phonon frequencies, and Davydov analysis.

References

(1) Smith, M. B.; Page, K.; Siegrist, T.; Redmond, P. L.; Walter, E. C.; Seshadri, R.; Brus, L. E.; Steigerwald, M. L. Crystal structure and the paraelectric-to-ferroelectric phase transition of nanoscale $BaTiO_3$. *J. Am. Chem. Soc.* **2008**, *130*, 6955–6963.

(2) Chattopadhyay, S.; Ayyub, P.; Palkar, V. R.; Multani, M. Size-induced diffuse phase transition in the nanocrystalline ferroelectric $PbTiO_3$. *Phys. Rev. B* **1995**, *52*, 13177–13183.

(3) Cho, D.; Cheon, S.; Kim, K.-S.; Lee, S.-H.; Cho, Y.-H.; Cheong, S.-W.; Yeom, H. W. Nanoscale manipulation of the Mott insulating state coupled to charge order in 1T-TaS_2. *Nat. Commun.* **2016**, *7*, 10453.

(4) Joseyphus, R. J.; Narayanasamy, A.; Shinoda, K.; Jeyadevan, B.; Tohji, K. Synthesis and magnetic properties of the size-controlled Mn-Zn ferrite nanoparticles by oxidation method. *J. Phys. Chem. Solids* **2006**, *67*, 1510–1517.

(5) Hung, C.-H.; Shih, P.-H.; Wu, F.-Y.; Li, W.-H.; Wu, S. Y.; Chan, T. S.; Sheu, H.-S. Spin-phonon coupling effects in antiferromagnetic Cr_2O_3 nanoparticles. *J. Nanosci. Nanotechnol.* **2010**, *10*, 4596–4601.

(6) Sun, Q. C.; Baker, S. N.; Christianson, A. D.; Musfeldt, J. L. Magnetoelastic coupling in bulk and nanoscale MnO. *Phys. Rev. B* **2011**, *84*, 014301.

(7) Chen, P.; Xu, X.; Koenigsmann, C.; Santulli, A. C.; Wong, S. S.; Musfeldt, J. L. Size-dependent infrared phonon modes and ferroelectric phase transition in $BiFeO_3$ nanoparticles. *Nano Lett.* **2010**, *10*, 4526–4532.

(8) Sun, Q. C.; Birkel, C. S.; Cao, J.; Tremel, W.; Musfeldt, J. L. Spectroscopic signature of the superparamagnetic transition and surface spin disorder in $CoFe_2O_4$ nanoparticles. *ACS Nano* **2012**, *6*, 4876–4883.

(9) Chen, Q.; Zhang, Z. J. Size-dependent superparamagnetic properties of $MgFe_2O_4$ spinel ferrite nanocrystallites. *Appl. Phys. Lett.* **1998**, *73*, 3156–3158.

(10) Amin, N.; Arajs, S. Morin Temperature of Annealed Submicronic α-Fe_2O_3 Particles. *Phys. Rev. B* **1987**, *35*, 4810–4811.

(11) Zysler, R. D.; Fiorani, D.; Testa, A. M.; Suber, L.; Agostinelli, E.; Godinho, M. Size dependence of the spin-flop transition in hematite nanoparticles. *Phys. Rev. B* **2003**, *68*, 212408.

(12) Yoo, K.; Jeon, B.-G.; Chun, S. H.; Patil, D. R.; Lim, Y.-J.; Noh, S.-H.; Gil, J.; Cheon, J.; Kim, K. H. Quantitative measurements of size-dependent magnetoelectric coupling in Fe_3O_4 nanoparticles. *Nano Lett.* **2016**, *16*, 7408–7413.

(13) Li, Z.-Q.; Zhang, L.; Song, Y.; Chen, X.-T.; Musfeldt, J. L.; Xue, Z.-L. Size-controlled synthesis and magnetic properties of copper germanate nanorods. Observation of size-induced quenching of the spin-Peierls transition. *CrystEngComm* **2014**, *16*, 850.

(14) Semeno, A. V.; Gilmanov, M. I.; Kuznetzov, A. V.; Melnik, N. N.; Grigorjeva, A. V.; Barulin, A. V.; Gudilin, E. A.; Demishev, S. V. The effect of spin-Peierls instability suppression in nanometer-scale-sized $CuGeO_3$ crystals. *Appl. Magn. Reson.* **2016**, *47*, 881–893.

(15) Hase, M.; Terasaki, I.; Uchinokura, K. Observation of the spin-Peierls transition in linear Cu^{2+} (Spin-$\frac{1}{2}$) chains in an inorganic compound $CuGeO_3$. *Phys. Rev. Lett.* **1993**, *70*, 3651–3654.

(16) Lussier, J.-G.; Coad, S. M.; McMorrow, D. F.; Paul, D. M. The temperature dependence of the spin-Peierls energy gap in $CuGeO_3$. *J. Phys. Condens. Matter* **1996**, *8*, 59–64.

(17) Martin, M. C.; Shirane, G. Temperature dependence of the spin-Peierls energy gap and anomalous line shapes in $CuGeO_3$. *Phys. Rev. B* **1996**, *53*, 713–716.

(18) Braden, M.; Wilkendorf, G.; Lorenzana, J.; Aín, M.; McIntyre, G. J.; Behruzi, M.; Heger, G.; Dhalenne, G.; Revcolevschi, A. Structural analysis of $CuGeO_3$: Relation between nuclear structure and magnetic interaction. *Phys. Rev. B* **1996**, *54*, 1105–1116.

(19) Els, G.; van Loosdrecht, P. H. M.; Lemmens, P.; Vonberg, H.; Güntherodt, G.; Uhrig, G. S.; Fujita, O.; Akimitsu, J.; Dhalenne, G.; Revcolevschi, A. Observation of Three-Magnon Light Scattering in $CuGeO_3$. *Phys. Rev. Lett.* **1997**, *79*, 5138–5141.

(20) Li, G.; Lee, J. S.; Long, V. C.; Musfeldt, J. L.; Wang, Y. J.; Almeida, M.; Revcolevschi, A.; Dhalenne, G. Far-infrared studies of spin-Peierls materials in a magnetic field. *Chem. Mater.* **1998**, *10*, 1115–1119.

(21) Takehana, K.; Oshikiri, M.; Takamasu, T.; Hase, M.; Kido, G.; Uchinokura, K. Magneto-optical measurements of $CuGeO_3$ in the far-infrared region. *J. Magn. Magn. Mater.* **1998**, *177-181*, 699–700.

(22) Takehana, K.; Takamasu, T.; Hase, M.; Kido, G.; Uchinokura, K. Far-infrared spectroscopy in the spin-Peierls compound $CuGeO_3$ under high magnetic fields. *Phys. Rev. B* **2000**, *62*, 5191–5198.

(23) Kiryukhin, V.; Keimer, B. Incommensurate lattice modulation in the spin-Peierls system $CuGeO_3$. *Phys. Rev. B* **1995**, *52*, 704–706.

(24) van Loosdrecht, P.; Boucher, J.; Martinez, G.; Dhalenne, G.; Revcolevschi, A. Inelastic light scattering from magnetic fluctuations in $CuGeO_3$. *Phys. Rev. Lett.* **1996**, *76*, 311–314.

(25) Lorenz, T.; Büchner, B.; Loosdrecht, P. H. M. V.; Schönfeld, F.; Chouteau, G.; Revcolevschi, A.; Dhalenne, G. Incommensurate Phase of $CuGeO_3$: From Solitons to Sinusoidal Modulation. *Phys. Rev. Lett.* **1998**, *81*, 148.

(26) Goñi, A. R.; Zhou, T.; Schwarz, U.; Kremer, R. K.; Syassen, K. Pressure-temperature phase diagram of the spin-Peierls compound $CuGeO_3$. *Phys. Rev. Lett.* **1996**, *77*, 1079–1082.

(27) Jayaraman, A.; Sharma, S. K.; Wang, S. Y.; Cheong, S.-W. Pressure-induced phases in the spin-Peierls compound $CuGeO_3$. *Phys. Rev. B* **1997**, *55*, 5694–5699.

(28) Nishi, M.; Kakurai, K.; Fujii, Y.; Yethiraj, M.; Tennant, D. A.; Nagler, S. E.; Fernandez-Baca, J. A.; Fujta, O.; Akimitsu, J. Magnetic excitation of $CuGeO_3$ under applied pressure. *Phys. B* **1998**, *241-243*, 537–539.

(29) van Loosdrecht, P. H. M.; Zeman, J.; Martinez, G.; Dhalenne, G.; Revcolevschi, A. Magnetic interactions and the pressure phase diagram of $CuGeO_3$. *Phys. Rev. Lett.* **1997**, *78*, 487–490.

(30) Damascelli, A.; van der Marel, D.; Parmigiani, F.; Dhalenne, G.; Revcolevschi, A. Infrared reflectivity of pure and doped $CuGeO_3$. *Phys. B* **1998**, *244*, 114–120.

(31) Damascelli, A.; van der Marel, D.; Dhalenne, G.; Revcolevschi, A. Optical spectroscopy of pure and doped $CuGeO_3$. *Phys. Rev. B* **2000**, *61*, 63–74.

(32) Poirier, M.; Beaudry, R.; Castonguay, M.; Plumer, M. L.; Quirion, G.; Razavi, F. S.; Revcolevschi, A.; Dhalenne, G. Doping effects on the magnetic phase diagram of the spin-Peierls system $CuGe_{1-x}Si_xO_3$. *Phys. Rev. B* **1995**, *52*, R6971.

(33) Kiryukhin, V.; Keimer, B.; Hill, J.; Vigliante, A. Soliton lattice in pure and diluted $CuGeO_3$. *Phys. Rev. Lett.* **1996**, *76*, 4608–4611.

(34) Völlenkle, H.; Wittmann, A.; Nowotny, H. Zur kristallstruktur von $CuGeO_3$. *Monatshefte für Chemie und verwandte Teile anderer Wissenschaften* **1967**, *98*, 1352–1357.

(35) Brill, T. M.; Boucher, J. P.; Voiron, J.; Dhalenne, G.; Revcolevschi, A.; Renard, J. P.

High-field electron spin resonance and magnetization in the dimerized phase of $CuGeO_3$. *Phys. Rev. Lett.* **1994**, *73*, 1545–1548.

(36) Braden, M.; Hennion, B.; Reichardt, W.; Dhalenne, G.; Revcolevschi, A. Spin-phonon coupling in $CuGeO_3$. *Phys. Rev. Lett.* **1998**, *80*, 3634–3637.

(37) Hirota, K.; Cox, D. E.; Lorenzo, J. E.; Shirane, G.; Tranquada, J. M.; Hase, M.; Uchinokura, K.; Kojima, H.; Shibuya, Y.; Tanaka, I. Dimerization of $CuGeO_3$ in the spin-Peierls state. *Phys. Rev. Lett.* **1994**, *73*, 736–740.

(38) Musfeldt, J. L.; Wang, Y. J.; Jandl, S.; Poirier, M.; Revcolevschi, A.; Dhalenne, G. Infrared investigation of the broken-symmetry ground state in $GeCuO_3$. *Phys. Rev. B* **1996**, *54*, 469–473.

(39) Li, G.; Musfeldt, J. L.; Wang, Y. J.; Jandl, S.; Poirier, M.; Revcolevschi, A.; Dhalenne, G. Optical observation of the interplay between magnetic and elastic energy in a spin-Peierls system. *Phys. Rev. B* **1996**, *54*, 633–636.

(40) Damascelli, A.; van der Marel, D.; Parmigiani, F.; Dhalenne, G.; Revcolevschi, A. Infrared signatures of the spin-Peierls transition in $CuGeO_3$. *Phys. Rev. B* **1997**, *56*, R11373–R11376.

(41) Nojiri, H.; Hamamoto, T.; Wang, Z. J.; Mitsudo, S.; Motokawa, M.; Kimura, S.; Ohta, H.; Ogiwara, A.; Fujita, O.; Akimitsu, J. Magnetic phase diagram and antiferromagnetic resonance in $CuGe_{1-y}Si_yO_3$. *J. Phys. Condens. Matter* **1997**, *9*, 1331–1338.

(42) Hase, M.; Terasaki, I.; Sasago, Y.; Uchinokura, K.; Obara, H. Effects of substitution of Zn for Cu in the spin-Peierls cuprate, $CuGeO_3$: The suppression of the spin-Peierls transition and the occurrence of a new spin-glass state. *Phys. Rev. Lett.* **1993**, *71*, 4059–4062.

(43) Masuda, T.; Fujioka, A.; Uchiyama, Y.; Tsukada, I.; Uchinokura, K. Phase transition between dimerized-antiferromagnetic and uniform-antiferromagnetic phases in the impurity-doped spin-peierls cuprate $CuGeO_3$. *Phys. Rev. Lett.* **1998**, *80*, 4566–4569.

(44) Dević, S. D.; Konstantinović, M. J.; Popović, Z. V.; Dhalenne, G.; Revcolevschi, A. Vibrational properties of copper metagermanate ($CuGeO_3$) single crystals. *J. Phys. Condens. Matter* **1994**, *6*, L745–L753.

(45) Popović, Z. V.; Dević, S. D.; Popov, V. N.; Dhalenne, G.; Revcolevschi, A. Phonons in $CuGeO_3$ studied using polarized far-infrared and Raman spectroscopies. *Phys. Rev. B* **1995**, *52*, 4185–4190.

(46) Popović, Z. V.; Stolz, H. J. Infrared and Raman spectra of germanium dichalcogenides I. GeS_2. *Phys. Status Solidi B* **1981**, *106*, 337–348.

(47) Chernyshova, I. V.; Hochella Jr., M. F.; Madden, A. S. Size-dependent structural transformations of hematite nanoparticles. 1. Phase transition. *Phys. Chem. Chem. Phys.* **2007**, *9*, 1736–1750.

(48) Okubo, M.; Hosono, E.; Kudo, T.; Zhou, H. S.; Honma, I. Phonon confinement effect on nanocrystalline $LiCoO_2$ studied with Raman spectroscopy. *J. Phys. Chem. Solids* **2008**, *69*, 2911–2915.

(49) Manciu, F. S.; Sahoo, Y.; Carreto, F.; Prasad, P. N. Size-dependent Raman and infrared studies of PbSe nanoparticles. *J. Raman Spectrosc.* **2008**, *39*, 1135–1140.

(50) Lee, C.; Gonze, X. Lattice dynamics and dielectric properties of SiO_2 stishovite. *Phys. Rev. Lett.* **1994**, *72*, 1686–1689.

(51) Savrasov, S. Y.; Kotliar, G. Linear response calculations of lattice dynamics in strongly correlated systems. *Phys. Rev. Lett.* **2003**, *90*, 056401.

(52) Simple changes in structure or stoichiometry would be expected to affect both infrared- and Raman-active modes equally. Although there are some differences in the XRD of the polycrystal and nanorods in the low angle region (Fig. S1 (c)), the structure is consistent within the nanorods. Synchrotron-based x-ray diffraction studies may reveal the exact structure of the nanorods.

(53) Davydov, A. S. The theory of molecular excitons. *Sov. Phys.* **1964**, *82*, 145–178.

(54) Popović, Z. V. Optical phonons in $SnGeS_3$. *Phys. Rev. B* **1985**, *32*, 2382–2387.

(55) Gasanly, N. M.; Faradzhev, F. E.; Ragimov, A. S.; Burlakov, V. M.; Goncharov, A. F.; Vinogradov, E. A. Davydov splitting and rigid-layer modes in InS crystal. *Solid State Commun.* **1982**, *42*, 843–845.

(56) Cross, M. C.; Fisher, D. S. A new theory of the spin-Peierls transition with special relevance to the experiments on TTFCuBDT. *Phys. Rev. B* **1979**, *19*, 402–419.

(57) Revcolevschi, A.; Dhalenne, G. Engineering oxide-oxide and metal-oxide microstructures in directionally solidified eutectics. *Adv. Mater.* **1993**, *5*, 657–662.

(58) Although the electronic structure does not vary greatly with size,[59] the phonons were not able to be resolved using the 532 nm laser for the two shortest nanorods. Instead, a 473 nm laser gave better spectra.

(59) O'Neal, K. R.; al-Wahish, A.; Li, Z.; Chen, P.; Kim, J. W.; Cheong, S.-W.; Dhalenne, G.; Revcolevschi, A.; Chen, X.-T.; Musfeldt, J. L. Vibronic coupling and band gap trends in $CuGeO_3$ nanorods. *Phys. Rev. B* **2017**, *96*, 075437.